Rapid diversification associated with a macroevolutionary pulse of developmental plasticity

Vladislav Susoy[1], Erik J. Ragsdale[1,2,*], Natsumi Kanzaki[3] & Ralf J. Sommer[1,*]

---

[1]Department of Evolutionary Biology, Max Planck Institute for Developmental Biology, Spemannstraße 37/4, 72076 Tübingen, Germany

[2]Department of Biology, Indiana University, 915 E. 3rd Street, Bloomington, IN 47405, USA

[3]Forest Pathology Laboratory, Forestry and Forest Products Research Institute, 1 Matsunosato, Tsukuba, Ibaraki 305-8687 Japan

*For correspondence: ragsdale@indiana.edu, ralf.sommer@tuebingen.mpg.de

Abstract

Developmental plasticity has been proposed to facilitate phenotypic diversification in plants and animals, but the macroevolutionary potential of plastic traits remains to be objectively tested. We studied the evolution of feeding structures in a group of 90 nematodes, including *Caenorhabditis elegans*, some species of which have evolved a mouthpart polyphenism, moveable teeth, and predatory feeding. Comparative analyses of shape and form, using geometric morphometrics, and of structural complexity revealed a rapid process of diversification associated with developmental plasticity. First, dimorphism was associated with a sharp increase in complexity and elevated evolutionary rates, represented by a radiation of feeding-forms with structural novelties. Second, the subsequent assimilation of a single phenotype coincided with a decrease in mouthpart complexity but an even stronger increase in evolutionary rates. Our results suggest that a macroevolutionary "pulse" of plasticity promotes novelties and, even after the secondary fixation of phenotypes, permits sustained rapid exploration of morphospace.

Main text

Developmental (phenotypic) plasticity has been proposed to affect evolution by facilitating adaptive change (Pigliucci, 2001; Schlichting, 2003; West-Eberhard, 2003; Moczek et al., 2011) but the relevant processes resulting in evolutionary diversity remain elusive. Identification of a switch gene for a dimorphism recently confirmed the link between developmental switches and microevolutionary divergence (Ragsdale et al., 2013), although insights from genetic mechanisms have yet to be put into a macroevolutionary context. For example, whether plasticity accelerates evolution by allowing faster evolutionary responses (Baldwin, 1896; Waddington, 1953; Suzuki and Nijhout, 2006) or hinders it by allowing adaptation without the need for genetic assimilation (Williams, 1966) is still a matter of debate (e.g. de Jong, 2005; Wund, 2012). To know the macroevolutionary potential of developmental plasticity, objectively measured plastic traits must be compared by deep taxon sampling in a robust phylogenetic framework. Here, we test the role of developmental plasticity in evolutionary tempo and novelty by measuring change in feeding structures in a group of 90 nematodes, including *Caenorhabditis elegans*, of which some species show a mouthpart polyphenism, moveable teeth, and predatory feeding. As a result we identified both the gain and loss of a developmental dimorphism to be associated with rapid evolutionary diversification. We made the surprising finding that whereas the appearance of polyphenism coincided with increased complexity and evolutionary rates, these rates were even higher after the assimilation of a single phenotype.

The evolutionary and ecological success of nematodes is reflected by the extensive adaptation of their feeding structures, including hooks and stylets in animal- and plant-parasitic nematodes and teeth in predatory species. The latter adaptation is found in the genetic model *Pristionchus pacificus* and other nematodes of the family Diplogastridae, in which cuticularized teeth and predation are sometimes associated with a dimorphism (Fürst von Lieven and Sudhaus, 2000). Dimorphic species execute either a “narrow-mouthed” (stenostomatous, St) or “wide-mouthed” (eurystomatous, Eu) morph, which differ in the size, shape, and complexity of their mouthparts (Figure 1). In *P. pacificus*, the St and Eu morphs are advantageous for feeding on bacteria and nematode prey, respectively (Serobyan et al., 2013, 2014). The dimorphism results from an irreversible decision during development, enabling a

rapid optimization of morphology to the environment (Bento et al., 2010). This response is mediated by small-molecule pheromones (e.g. dasc#1, ascr#1) (Bose et al., 2012), endocrine signaling (dafachronic acid-DAF-12) (Bento et al., 2010), and a switch mechanism executed by the sulfatase EUD-1 (Ragsdale et al., 2013).

To study the tempo and mode of evolution in nematode mouthparts, we analyzed 54 species of Diplogastridae, 23 of which we found to be dimorphic. The remaining 31 diplogastrid species were identified as monomorphic. We also analyzed 33 species of other Rhabditina (De Ley and Blaxter, 2002), which include *C. elegans* and the closest known outgroups of Diplogastridae (Kiontke et al., 2007; van Megen et al., 2009). In contrast to Diplogastridae, all non-diplogastrid Rhabditina were monomorphic.

To test whether the dimorphism where present was a polyphenism, and not the result of genetic polymorphism (Schwander and Leimar, 2011), we exposed dimorphic species to cues potentially regulating their dimorphism. For assays we selected systematically inbred or genetically bottlenecked phylogenetic representatives. When exposed to signals of starvation, crowding, or the presence of nematode (*C. elegans*) prey, all species tested produced a higher number of Eu individuals in response ($P < 10^{-6}$, Fisher's exact test, for all induction experiments; Table 1, Table 1-source data 1). Thus, alternative conspecific morphs are the result of polyphenism across taxa of Diplogastridae.

To determine the order and directionality of changes in mouthpart evolution, we inferred the phylogeny of Diplogastridae and outgroups using 14 genes in an alignment of 11,923 total and 6354 parsimony-informative sites (Figure 2A). Because our analysis included many taxa previously not analyzed by any molecular characters, newly inferred and highly supported relationships among taxa allowed robust inferences of ancestral states. The inferred history of the mouth dimorphism revealed that it evolved once but was lost at least 10 times, and possibly 11 given the ambiguous position of *Leptojacobus dorci* (Figure 2A). Thus, the morphological diversity of diplogastrid mouthparts (Figure 2B) represents a radiation that accompanied the origin of polyphenism in those structures and involved many independent transitions to a monomorphic phenotype.

Next, we wanted to know whether the radiation of mouthparts in Diplogastridae that had dimorphism in their history represented a measurable increase in morphological variance with respect to outgroups. We quantified mouth morphology

by recording 11 geometric landmarks of the stoma that were considered homologous, as informed by fine-structural anatomy, across Diplogastridae and outgroups (Baldwin et al., 1997; Ragsdale and Baldwin, 2010) (Figures 1A,B, 3A). Analysis of landmark coordinates in Procrustes space for shape and form, the latter including shape + log-transformed centroid size (Dryden and Mardia, 1998; Mitteroecker et al., 2004), showed that non-diplogastrid Rhabditina occupy only a subset of the total morphospace colonized by Diplogastridae (Figure 3A, Figure 3-figure supplement 1, Figure 3-source data 1-4). This represented greater disparity for Diplogastridae than for non-diplogastrid Rhabditina, whether disparity was measured as the sum of variances ($P < 10^{-5}$ when either St or both morphs represented dimorphic taxa) or by principal component analysis (PCA) volume (Ciampaglio et al., 2001) (Figure 3B, Figure 3-source data 5). However, the disparity for either morph of dimorphic taxa was not different from that of non-diplogastrid Rhabditina. In contrast, diplogastrids that were secondarily monomorphic showed higher disparity than either morph in dimorphic taxa ($P < 0.02$ for both) (Figure 3B, Figure 3-source data 5). Taken together, these findings show clear disparity differences between non-diplogastrid Rhabditina, dimorphic Diplogastridae, and secondarily monomorphic Diplogastridae.

We next tested if the observed morphospace occupation differences within Diplogastridae and across Rhabditina reflected shifts in evolutionary tempo, specifically with the gain or loss of the mouth polyphenism. Using the inferred phylogenies we measured the rate of change in shape and form (PC1) as a Brownian rate parameter under one-, two-, and three-rate parameter models (O'Meara et al., 2006). We found that the two-rate model that approximated different rate parameters for non-diplogastrid Rhabditina and Diplogastridae was favored over the single-rate model for both form (ΔAICc = 5.34; $P = 0.01$) and shape (ΔAICc = 11.71; $P < 0.001$, likelihood ratio test), with rates in Diplogastridae being higher (Figure 3C,D, Figure 3-figure supplement 2, Figure 3-source data 6, 7). Furthermore, a three-rate model that assumed a different rate parameter for each of the three nematode groups had the greatest fit compared with either a single-rate model (ΔAICc = 9.18, $P = 0.038$ for form; ΔAICc = 14.79, $P < 0.001$ for shape) or a model that assigned a different rate category to dimorphic diplogastrids (ΔAICc = 9.32, $P < 0.01$ for form; ΔAICc = 15.27, $P < 0.001$ for shape), and rates in monomorphic Diplogastridae were the highest (Figure 3C). For form evolution in particular, a two-rate model that assumed a different rate parameter for monomorphic Diplogastridae was a better fit than all other

models, including that with a single category for Diplogastridae (ΔAICc = 5.23). Congruent with these results, a comparison of posterior densities of rate estimates from the Bayesian sampling of a multirate Brownian-motion process (Eastman et al., 2011), which were extracted for individual nematode groups, indicated elevated rates of evolution in Diplogastridae relative to non-diplogastrid Rhabditina, with rates in secondarily monomorphic lineages being the fastest (Figure 3-figure supplement 3, Figure 3-source data 8). Thus, our analyses of evolutionary rates show that diversification of shape and form in Diplogastridae increased with the appearance of the mouth plasticity but were highest after its subsequent loss.

We then wanted to know whether developmental plasticity also correlated with the complexity of mouthparts that distinguishes Diplogastridae from their closest relatives (Figure 2B). We tabulated complexity for all taxa by recording the number of stomatal structures or "cusps," adapting a concept of complexity commonly applied to the dentition of vertebrates (Harjunmaa et al., 2012). Namely, we scored all structures or articulations that formed a <135º vertex with the wall of the stoma (Figure 4-figure supplement 1, Figure 4-source data 1), summing the total to an index that was invariable for all specimens of a given species or, in dimorphic species, a particular morph (here, Eu). We then tested for phylogenetic correlations of this complexity index with the presence of plasticity. Plasticity was strongly correlated with greater complexity, as shown by their covariance tested either under the threshold model (Felsenstein, 2012) (r = 0.78, confidence interval 0.57-0.93) or a constant-variance random-walk model (r = 0.45; log Bayes factor = 20). Given the character histories of known taxa (Figure 4), this result reveals that the gain of the polyphenism was simultaneous with the onset of high complexity, including the origin of opposable teeth. In contrast, the loss of the polyphenism in monomorphic Diplogastridae was associated with a subsequent decrease in complexity.

Our results provide original statistical and phylogenetic support for a role of developmental plasticity in evolutionary diversification. They are also congruent with a simple model for the role of plasticity in this process. First, the appearance of bimodal plasticity coincides with a burst of complexity and increase in evolutionary tempo. By this model, developmental plasticity can facilitate novel structures and their associated developmental networks (West-Eberhard, 2003), as well as new complexity in behavioral or enzymatic function, thereby providing additional substrate for future selection. Following this macroevolutionary "pulse" of plasticity,

178 the secondary loss of plasticity is accompanied by a decrease in complexity but a
179 strong acceleration of measured evolutionary rates, which in our study were most
180 pronounced in form change. The surprising limitation of rates in dimorphic relative to
181 secondarily monomorphic lineages might be explained in part by genetic correlation
182 (Cheverud, 1996), or the inability of overlapping genetic programs controlling
183 alternative phenotypes to completely dissociate. We speculate that, where correlated
184 morphologies were initially governed by a dimorphism, assimilation of a single
185 morph would then give the freedom for single phenotypes to specialize and diversify,
186 a phenomenon proposed as developmental "character release" (West-Eberhard, 1986).
187 A complementary means by which evolutionary rates increase after the loss of
188 plasticity may be through the release of genetic variation built up as a by-product of
189 relaxed selection (Kawecki, 1994; Snell-Rood et al., 2010; Van Dyken and Wade,
190 2010). This possibility might be realized through the following scenario. If
191 populations experience fluctuating environments and alternative mouth morphologies
192 confer fitness advantages in those environments, then environmental sensitivity (i.e.
193 plasticity) will be maintained (Moran, 1992). The presence of plasticity necessarily
194 leads to relaxed selection on genes underlying the production of either trait,
195 particularly those downstream of a developmental switch, facilitating the
196 accumulation of genetic variation (Van Dyken and Wade, 2010). If populations then
197 encounter a stable, predictable environment, promoting the loss of plasticity
198 (Schwander and Leimar, 2011), this variation can be selected and refined by
199 constitutively exposing a single morph to that environment. This would allow more
200 rapid evolution of novel phenotypes than would be possible through the generation
201 and selection of new genetic variation (Barrett and Schluter, 2008; Lande, 2009),
202 thereby allowing rapid shifts to alternative niches such as novel diets (Ledón-Rettig et
203 al., 2010). Combined with the ability of fixed morphs to more efficiently reach their
204 fitness optima as permitted by character release, variation accumulated during periods
205 of plasticity would thus enable rapid phenotypic specialization and diversification.
206 Although accelerated rates of divergence due to built-up variation and character
207 release should ultimately decline in monomorphic lineages (West-Eberhard, 2003;
208 Lande, 2009), the net result would be an extreme radiation of forms, as has occurred
209 in diplogastrid nematodes.
210 In conclusion, the historical presence of polyphenism is strongly associated with
211 evolutionary diversification. The degree to which the correlations observed are due to

causation is presently unclear, although recent mechanistic advances in *P. pacificus* demonstrate the promise of functional genetic studies to test the causality of rapidly selected genes directly. Further work might also reveal that additional underlying causes, such as previously unseen ecological opportunities or selective pressures, may have jointly led to both complexity and plasticity. However, the simplicity of our results makes our proposed model sufficient to explain the observed correlations. We therefore hypothesize that developmental plasticity is required to cross a threshold of complexity that affords the degrees of freedom necessary for further diversification of form, and even after the assimilation of monomorphy this diversification can continue to be realized. The difference in rates between ancestrally and secondarily monomorphic lineages suggest a deciding role for a history of plasticity in diversification. It is possible that the processes inferred to accompany the gain of plasticity apply also to other systems with taxonomically widespread polyphenism, which sometimes likewise show a general coincidence of plasticity and diversity (e.g. Emlen et al., 2005; Pfennig and McGee, 2010). In principle, the model we propose can be generalized to other systems through dense taxon sampling, a resolved phylogeny, and quantification of alternative morphologies.

Acknowledgements

We thank Waltraud Röseler, Aziza Aust, and Hanh Witte for helping with DNA preparation, Matthias Herrmann for help with nematode collecting, and Robin Giblin-Davis for providing several nematode strains.

Author contributions

VS, Conception and design, Sample collection, Acquisition of data, Performed experiments, Analysis and interpretation of data, Wrote the manuscript

EJR, Conception and design, Acquisition of data, Interpretation of data, Wrote the manuscript

NK, Sample collection, Acquisition of data

RJS, Sample collection, Wrote the manuscript

For correspondence

ragsdale@indiana.edu (EJR)

ralf.sommer@tuebingen.mpg.de (RJS)

Competing interests

The authors declare that no competing interests exist.

Funding

Max Planck Society

- Ralf J Sommer

The funder had no role in study design, data collection or interpretation, or the decision to submit the work for publication.

Materials and Methods

Nematodes

To investigate evolutionary rates, complexity, and character histories, we densely sampled nematodes of Rhabditina *sensu* De Ley & Blaxter (2002) (= Clade V *sensu* Blaxter et al., 1998). Isolation details for all analyzed nematode taxa for which original sequence data were obtained are given in Figure 2-source data 1. Our taxonomic nomenclature follows previous systems (Andrássy, 1984, 2005; Sudhaus and Fürst von Lieven, 2003) with additional genera described since those publications (Ragsdale et al., 2014). Our dataset included 54 species of Diplogastridae, in addition to 33 nematode species from all closest known outgroups to the family: "Rhabditidae" *sensu* Sudhaus (2011), Brevibuccidae, Bunonematidae, Myolaimidae, and Odontopharyngidae. In the present study, "non-diplogastrid Rhabditina" refers to the latter five families together. Rhabditidae were sampled such that they spanned all major clades of that group as identified in a previous study (Kiontke et al., 2007): the *Mesorhabditis* group and non-*Mesorhabditis* "pleiorhabditids"; *Caenorhabditis*, the four deepest lineages of the *Rhabditis* group, and the remaining two deepest lineages of "eurhabditids"; *Rhabditoides inermis*, a possible immediate outgroup to Diplogastridae; *Poikilolaimus*, the putative sister group to all other Rhabditidae and nested taxa. Three Clade IV (Blaxter et al., 1998) nematode species were included as outgroups in the dataset.

Phylogenetics

Dataset assembly. The phylogeny of Diplogastridae was inferred from concatenated alignments of 18S and 28S rRNA genes and 11 ribosomal protein-coding genes of 90 taxa. Genomic DNA was extracted from individual specimens and total RNA from 15-45 individuals per species (Figure 1-source data 2). Genes of interest were amplified individually, and sequencing reactions were performed as previously described (Mayer et al., 2009). Sequences were assembled using Geneious 6.1.4. Sequences for 18S, 28S, ribosomal protein, and RNA polymerase II genes, which were either original in this study or retrieved from public databases, were included for non-diplogastrid Rhabditina and outgroups. 18S and 28S rRNA sequences were aligned using the E-INS-I algorithm and default settings in MAFFT 7.1 (Katoh and Standley, 2013). Alignments were manually refined, and poorly aligned regions were eliminated

manually. Alignments of 18S and 28S rRNA genes were 1598 and 3155 bp long, respectively, and included 859 and 1616 parsimony-informative sites. Sequences of each of the 11 ribosomal protein genes were aligned individually using default settings in Muscle 3.8 (Edgar, 2004) and were realigned by predicted translation; alignments were manually refined and stop-codon sites removed. The concatenated alignment of 11 ribosomal protein genes was 5475 bp long and included 2970 parsimony-informative positions. Aligned sequences for Diplogastridae contained 444 kb without missing data. The final dataset of diplogastrid sequences was more than four times larger than that used in the previously most inclusive phylogenetic study of the family (Mayer et al., 2009), and it included over three times as many species and twice as many diplogastrid genera. In the final concatenated alignment of rRNA and ribosomal protein genes for all diplogastrid species, the proportion of missing data was 20%, with a minimum of 70% of nematode species sampled per gene. The dataset of all taxa had 667 kb excluding missing data and was 11,923 bp long (Supplementary file 1), in which the fraction of missing data was 38%.

Inference methods. The phylogeny was inferred under Bayesian and maximum likelihood (ML) optimality criteria as implemented in MrBayes 3.2.2 (Ronquist et al., 2012) and RAxML 7.3 (Stamatakis, 2006), respectively. All inferences were performed on the CIPRES Science Gateway (Miller et al., 2006). For Bayesian inference, the dataset was partitioned into four subsets: two for 18S and 28S rRNA genes, which were analyzed using a "mixed" + Γ model, and the third and fourth for the combined ribosomal protein genes and RNA polymerase II, respectively, which were analyzed under a codon + Γ model. Model parameters were unlinked across partitions. Four independent analyses, each containing four chains, were run for 55 million generations, with chains sampled every 1000 generations. After confirming convergence of runs and mixing of chains using Tracer 1.6 (Drummond and Rambaut, 2007), the first 50% generations were discarded as burn-in and the remaining topologies summarized to generate a 50% majority-rule consensus tree. For the ML analysis, our partitioning scheme divided the dataset into three subsets: two for the 18S and 28S rRNA genes, which were each analyzed using a GTR + Γ model, and the third subset for translated ribosomal protein and RNA polymerase II genes, analyzed under an inverse-gamma (IG) + Γ model. The latter model was selected based on an amino-acid substitution-model test as implemented ProtTest 3 (Darriba et al., 2011). 100 independent ML searches initiated with random starting trees were performed.

Support values for the best-scoring tree were estimated from 1000 iterations of non-parametric bootstrapping.

Presence of polyphenism

We identified nematode species as dimorphic or monomorphic by screening at least two hundred individuals in cultured populations under both well-fed and starved conditions, the latter of which is known to induce the Eu morph in *P. pacificus* (Bento et al., 2010). Dimorphism was diagnosed by the presence of morphs that differed (i) in the width and aspect ratio of the stoma and (ii) in the prominence and sclerotization of mouth structures (Fürst von Lieven and Sudhaus, 2000; Serobyan et al., 2013). In all examined species with mouth plasticity, the plasticity was discrete with no observed (and hence presumably rare) intermediate forms or reaction norms for morph-diagnostic morphology. Furthermore, each of the two morphs was stereotypic for a given species, such that morphology did not qualitatively vary with different induction cues. The mouth plasticity was therefore a discrete dimorphism of constant morphs in all species with the plasticity, consistent with previous observations of *P. pacificus*, for which multiple levels of starvation, pheromones, hormones, transgenes, enzyme-inhibiting salts, or environments previously experienced by wild-caught specimens all induced either of two morphs, albeit in differing ratios (Bento et al., 2010; Bose et al., 2012; Ragsdale et al., 2013; Serobyan et al., 2013). For species that could not be brought into culture (annotated as "nc" in Figure 2-source data 1), all of which were monomorphic, observations of collected isolates were corroborated by comprehensively reviewed previous taxonomic studies (Sudhaus and Fürst von Lieven, 2003) to confirm the absence of dimorphism. Taken together, previous reports and our own collections demonstrated that such species were monomorphic across multiple populations and environmental conditions. In each of the five cases of recent losses, namely those inferred to have occurred on a terminal branch within Diplogastridae, the assimilated morph was identified as the St morph. However, for inferred ancient losses of the dimorphism, derived morphology made the homology of the assimilated morph impossible to determine reliably. Therefore, our analyses identify monomorphic and dimorphic taxa without distinguishing which of the two morphs was lost or assimilated.

Environmental induction of alternative morphs. To test whether the mouth dimorphism of diplogastrid nematodes was an environmental polyphenism and not

genetic polymorphism, we exposed dimorphic species to environmental conditions potentially influencing expression of the two alternative mouth phenotypes. Specifically, we tested species (strains) with high frequency of St morph for environmental induction of the Eu morph. Although all strains tested had been kept in laboratory culture for at least one year prior to experiments, several strains (*Allodiplogaster sudhausi*, both *Micoletzkya* spp., *Parapristionchus giblindavisi*) were additionally inbred systematically for 10 generations.

In our first assay (Table 1-source data 1), 7 fertile St females or hermaphrodites (5 for *Allodiplogaster sudhausi*) were transferred from a stock culture well-fed with bacteria onto an NGM plate (no peptone, no cholesterol) supplied with approximately 70,000 to 100,000 arrested *C*. *elegans* larvae. In parallel, the same number of St females or hermaphrodites was transferred onto NGM plates with the same species of bacteria as that on stock culture plates: this was OP50 for most species, although some species (i.e. *Micoletzkya* spp.) required different bacterial strains to reproduce. Nematodes were allowed to feed on the provided food, lay eggs, and develop in the following generation. The mouth phenotype of all F1 females or hermaphrodites was scored when those individuals reached adulthood (5 to 10 days, depending on the species). Experiments were performed in triplicate for each species.

Because some species could not develop in the absence of microbial food, we employed a second strategy to test for environmental induction of the Eu morph in those strains. In this assay (Table 1-source data 1), 10 to 15 fertile females were transferred to plates seeded with a 500 µl bacterial lawn. After the time necessary for the populations of a species to complete one generation following the visible depletion of a bacterial lawn (*Diplogasteriana* n. sp., 6 weeks; *Koerneria luziae*, 2.5 weeks; *P*. *giblindavisi*, 2 weeks), adult females were screened for their mouth phenotype. In parallel, nematodes of the same species were maintained in well-fed culture, being transferred (10 to 15 females per replicate) to a new bacterial lawn, the next generation being screened for the mouth phenotype after one week. All adult females up to a sample size of 200 per plate were screened. Experiments were performed in triplicate for each species.

For both assays, significant differences in morph ratios between prey-fed and bacteria-fed nematodes were calculated using Fisher's exact test with the total number of assayed individuals pooled across replicates. Effect sizes of differences were

393 estimated as the odds ration by Fisher's exact test. The percentage of the Eu morph per
394 treatment per species is reported in Table 1 for pooled samples.
395
396 **History of dimorphism**
397 To infer the evolutionary history of the stomatal dimorphism, we used stochastic
398 character mapping (Nielsen, 2002; Huelsenbeck et al., 2003) as implemented in
399 SIMMAP 1.5 (Bollback, 2006). This approach estimates probabilities of the states
400 along phylogeny under continuous-time Markov models, incorporating uncertainty in
401 tree topology, branch length, and ancestral character states. The best-fitting parameters
402 of morphology priors, the overall substitution rate prior (gamma distribution prior),
403 and the bias prior for two-state characters (beta distribution prior) were estimated
404 using a Markov-chain Monte Carlo (MCMC) method as also implemented in
405 SIMMAP. These calibration analyses were run for 500,000 generations, sampling the
406 chain every 100 generations, using a 50% majority rule consensus tree summarized
407 from the Markov chains of the Bayesian phylogenetic analysis; the first 50,000
408 generations were discarded as burn-in. For stochastic character mapping, 500 trees
409 were randomly sampled, with the help of Mesquite 2.75 (Maddison and Maddison,
410 2011), from trees generated during the MCMC runs. The number of discrete
411 categories, *k*, was set to 90 and 31 for the gamma and beta distributions, respectively.
412 Trees were rescaled to a length of one before applying priors on the overall rate. For
413 analyses of evolutionary rates and complexity correlation, 10 character histories were
414 simulated on each of the 500 trees. The density maps of the dimorphism history
415 (Figures 2A, 3E) were generated by summarizing posterior densities from 500
416 simulations of character histories on the ML tree in the R package phytools 0.3-72
417 (Revell, 2012).
418
419 **Geometric morphometrics**
420 To capture stomatal morphology, 11 fixed two-dimensional landmarks were placed at
421 locally defined boundaries or points within the stoma (Figure 3A). Landmarks
422 consisted of boundaries or points that were considered homologous across Rhabditina
423 as predicted by fine-structural anatomy (Baldwin et al., 1997; Ragsdale and Baldwin,
424 2010); stomatal terminology follows De Ley et al. (1995). Type-1 landmarks were
425 recorded at the ventral and dorsal boundaries of the cheilostom with labial tissue
426 (landmarks 1 and 11, respectively), the ventral and dorsal boundaries between the

cheilostom and gymnostom (2 and 10, respectively), the ventral and dorsal boundaries between the gymnostom and stegostom (4 and 8, respectively), the posterior boundary of the dorsal telostegostom (6), and the dorsal gland orifice (7); type-2 landmarks included the anterior apex of the ventral and dorsal gymnostom (3 and 9, respectively) and the apex of medial curvature of the subventral telostegostom (5). To exclude contribution of the third dimension to morphometrics, all landmarks were recorded in exactly lateral view, as guaranteed by the body habitus of slide-mounted nematodes, i.e. their sinusoidal spread along the sagittal plane.

For 68 nematode species, landmarks were recorded for multiple live specimens, which were mounted on 5% agar pads with 8 µl of 0.25 M sodium azide added as an anesthetic. Microscopy was performed using a Zeiss Axio Imager.Z1 equipped with a Spot RT-SE digital camera. Landmark positions were marked using live-view mode in Metamorph 7.1.3 (Molecular Devices, Sunnyvale, CA, USA), and after image acquisition they were digitalized using tpsDig2 (Rohlf, 2008). For 22 species, we used video vouchers and images from published sources for digitalization of landmarks. Our complete morphometric dataset consisted of 522 images and 90 nematode species (an average of 4.8 images per species or morph). Landmark positions and centroid sizes (square root of the sum of squared distances of landmarks to their centroid) were averaged for each species (or each morph for dimorphic species), whereafter landmarks were Procrustes-superimposed using MorphoJ (Klingenberg, 2011).

We used two approaches to analyze landmarks. First, we simultaneously accounted for variation in both stomatal shape and size by performing Procrustes form-space (size-shape space) analyses (Dryden and Mardia, 1998; Mitteroecker et al., 2004). In this approach, Procrustes shape coordinates, which are the result of landmark centering, rotation, and scaling, are augmented by the natural-logarithm-transformed centroid size (i.e. as calculated prior to scaling) and subjected to principal component analysis (PCA). PCA on the Procrustes shape coordinates matrix was performed with an additional column appended containing log-transformed centroid size data using the "prcomp" function in R 3.0.2 package Stats (R Development Core Team, 2013). In the second approach, we performed PCA analysis on Procrustes shape coordinates to reconstruct Procrustes shape-space (Rohlf and Slice, 1990). In contrast to form-space, shape-space in principle minimizes the effects of allometry, offering an alternative way to measure morphological change. When data for all species and morphs were combined (Figure 3A), the first and the second PC axes of form-space accounted for

approximately 73% and 16% (68% and 12% for shape-space), respectively, of the variance. Thus, the cumulative proportion of the overall variance explained by PC1 and PC2 axes was 88% and 81% for form- and shape-space, respectively (Figure 3-source data 1, 2). In form-space analyses, loadings of the log centroid size onto PC1 and PC2 axes were 0.91 and 0.41 (Figure 3-source data 1, 2).

In addition to the PCA above, we performed phylogenetic PCA on both form and shape matrices for evolutionary rate analyses (Revell, 2009) to account for phylogenetic non-independence of morphometric data. The St morph represented dimorphic species in this PCA (Figure 3-source data 3, 4). Disparity analyses included several components of the standard PCA were retained (see below). All other analyses, which comprised phylogenetically corrected inference and tests of evolutionary rates requiring individual variables, used scores along the first PC axis of each phylogenetic PCA and which explained the vast majority of variance in either form or shape.

Disparity

Morphological variation (disparity) was examined in three groups, namely non-diplogastrid Rhabditina, dimorphic Diplogastridae, and monomorphic Diplogastridae. We used two approaches to investigate disparity: (i) the sum of univariate variances on form-space axes (multivariate variance) and (ii) PCA volume (Figure 3-source data 5). These methods capture different aspects of morphological diversity and both are based on morphological distance measures, although neither controls for phylogenetic non-independence. The sum of variances, a variance-based metric, provides an estimate of degree of difference among species in Procrustes morphospace. Alternatively, PCA volume gives an estimate of the amount of morphospace occupied by species; it is calculated as the product of the eigenvalues of the cross-distance matrix, divided by the square of the number of species. The sum of variances was previously shown by simulation-based studies to be relatively insensitive to variation in sample size, and both methods have relatively low sensitivity to missing data (Ciampaglio et al., 2001). The analyses were performed using the MATLAB package MDA (Navarro, 2003). PC axes that explained more than 5% of the overall variance (2 for form, 3 for shape) (Figure 3-source data 1, 2) were retained for calculations of the sum of variances and PCA volume. Rarefaction was performed to correct for sample-size dependence (Ciampaglio et al., 2001), such that the sample size was standardized to the number of species in the smallest group compared. To calculate means of disparity estimates,

their standard deviations, and their 95% confidence intervals, 10,000 bootstrap replicates were performed. For pairwise comparisons of the sum of variances between groups, two-tailed p-values were estimated using 100,000 bootstrap replicates.

Evolutionary rates

We used two comparative methods that employ a Brownian motion (BM) model to estimate and compare rates of evolution of stomatal morphology among different nematode lineages: (i) a ML-based non-censored rate test (O'Meara et al., 2006) and (ii) a Bayesian reversible-jump approach (Eastman et al., 2011). In these approaches, the rate of evolution is measured as a rate parameter for the BM process by weighting the magnitude of change of the trait per unit of "operational time" (Pagel, 1997). In our analyses, operational time was set to inferred genetic distance, i.e. branch lengths inferred in our Bayesian phylogenetic analysis of four partitions of the 14 included genes. This metric is supported as an appropriate measure of time by mutation accumulation line experiments, which have indicated rates of molecular evolution to be nearly identical between distantly related nematodes of Rhabditina (Weller et al., 2014). Absolute time was not used because (i) relevant fossil data are not available to calibrate dates in the phylogeny and (ii) the number of generations per year is assumed to differ dramatically between nematode species due to differences in generation time and, given ecological differences (Herrmann et al., 2006; Kiontke et al., 2011), presumed lengths of diapause (dauer) stages.

Non-censored rate test. To investigate how rates of morphological (form and shape) evolution change in the presence of plasticity, we estimated the relative fit of one-, two-, and three-rate parameter models using the "Brownie.lite" function in the R package phytools 0.3-72 (Revell, 2012) (Figure 3-source data 6). Five BM models were tested: (i) a single rate model that approximated the same rate parameter for non-diplogastrid Rhabditina, dimorphic Diplogastridae, and monomorphic Diplogastridae (1,1,1 model); (ii) a two-rate parameter model that assigned one rate category to non-diplogastrid Rhabditina and a different category to dimorphic and monomorphic Diplogastridae together (1,2,2 model); (iii) a two-rate model that approximated one rate parameter for non-diplogastrid Rhabditina and monomorphic diplogastrids but a different rate parameter for dimorphic Diplogastridae (1,2,1 model); (iv) a two-rate model that assumed the same rates for non-diplogastrid Rhabditina and dimorphic Diplogastridae but different rates for monomorphic Diplogastridae (1,1,2 model); (v) a

three-rate model that assumed different rate parameters for each of the three nematode groups (1,2,3 model). We assessed the relative fit of models by comparing second-order Akaike Information Criterion (AICc) values (Figure 3-source data 6). If the difference in values (ΔAICc) was greater than 4, the worse-fitting model was considered much less supported (Burnham and Anderson, 2002). Additionally, nested models were compared using a hypothesis-testing likelihood-ratio approach, i.e. using a chi-square distribution (Figure 3-source data 7; p-values are also given in main text). Tests were performed on 5,000 trees with mapped character histories, which were randomly sampled from posterior distributions of post-burn-in trees generated by the MCMC runs of the phylogenetic analysis.

Bayesian sampling of shifts in trait evolution. We investigated variation in evolutionary rates across lineages of Rhabditina using a Bayesian reversible-jump approach (Eastman et al., 2011) as implemented in the R package Geiger 1.99-3 (Harmon et al., 2008) (Figure 3-source data 8). This method estimates posterior rates of continuous trait evolution along individual branches of the phylogeny using reversible-jump MCMC sampling of a multirate BM process, without the need for specifying hypotheses *a priori* about the location of rate shifts. To achieve mixing of MCMC chains, we calibrated the proposal width using the function "calibrate.rjmcmc" and running the chain for 1 million generations, after which we used Tracer 1.6 to confirm mixing. Three MCMC analyses were then performed, with 30 million generations each, using the function "rjmcmc.bm." Analyses were run under a relaxed-BM model with the number of local clocks constrained to three and the proposal width set to 1.5. Chains were sampled every 5000 generations, the first 25% of generations was discarded as burn-in, and Tracer 1.6 was used to confirm chains mixing and convergence. Results from the three independent runs were combined, and weighted posterior rates of individual branches within each of the compared categories were extracted. The highest posterior density (HPD) intervals and means were estimated for the three nematode groups (Figure 3-figure supplement 3) and were compared using a two-tailed randomization test to determine whether posterior rates were different among groups (Figure 3-source data 8).

Dimorphism and stomatal complexity

Tabulating complexity. To establish an index for the complexity of nematode mouthparts, we scored the total number of observed cuticular “cusps” (Harjunmaa et

al., 2012) and articulations, i.e. structures projecting independently within the stoma. We define a "structure" herein as any geometric deviation that is marked by a physical vertex of <135º from the cylindrical walls of the stoma or from the arched anterior margins of the pharyngeal radii (Figure 4-figure supplement 1). All recorded structures were discrete and stereotypic, i.e. always present or absent, for each species or morph (for dimorphic taxa, the Eu morph was analyzed). Because such structures take a variety of shapes, all recorded structures are for clarity presented as a presence/absence character matrix (Figure 4-source data 1), which includes structures consistent with previous reports (Fürst von Lieven, 2000; Fürst von Lieven and Sudhaus, 2000; Sudhaus and Fürst von Lieven, 2003; Kanzaki et al., 2012; Herrmann et al., 2013; Ragsdale et al., 2014). Iterative structures (i.e. serratae, rods, points, warts, serial denticles, and divisions of stomatal wall) were conservatively scored as a single structure, because such iterative structures were always co-dependent and were sometimes (i.e. for denticles, serratae, and warts) variable in number among individuals of a single species. Furthermore, such structures show that this additional within-character complexity correlates with size, analogous to what is observed in mammalian tooth development (Harjunmaa et al., 2014) or what might otherwise be expected in area-dependent patterning (Turing, 1952). Therefore, to minimize the effects of size on complexity in our analyses, all tabulated structures were those that were unique and constant within a species and which could be assigned homology where present in multiple species. Additionally, structures that bore multiple vertices or "secondary complexity" distal to its deviation from the stoma (i.e. teeth, which could have multiple bends or peaks) were also coded as single structures. Finally, any character present as identical, symmetrical duplicates, which was due to the presence of two subventral sectors and hence also developmental co-dependence, was scored as a single structure. Examples of stomata with all of their structures recorded and labeled are shown in Figure 4-source data 1.

All Diplogastridae and some non-diplogastrid Rhabditina were observed by differential interference contrast (DIC) microscopy. For other taxa, morphology was scored from published DIC video vouchers, DIC micrographs, and drawing interpretations; stomatal morphology for genera of Rhabditidae was additionally confirmed according to a recent key for the family (Scholze and Sudhaus, 2011). Observed structures comprised a total of 25 characters. For the set of analyzed taxa, the complexity index ranged from 0 to 9.

Character correlation. We tested for a correlation between presence of mouth dimorphism and stomatal complexity using the dataset that included all 87 species of Rhabditina and the threshold model (Felsenstein, 2012) as implemented in the R package phytools 0.3-72 (Revell, 2012). We ran 50 analyses of 500,000 generations each and using trees randomly sampled from the posterior distributions of trees generated by the phylogenetic analysis in MrBayes 3.2.2. After confirming chain convergence and discarding 25% of the posterior samples as burn-in, the outputs of the analyses were combined and used to calculate the maximum likelihood estimation of the correlation coefficient. The R package coda 0.16-1 (Plummer et al., 2012) was used to compute the highest posterior density intervals of those estimates. Additionally, we tested for correlation between dimorphism and stomatal complexity by Bayesian MCMC sampling as implemented in BayesTraits V2 (beta) (Pagel and Meade, 2013). For this test, a constant-variance random-walk model was invoked. The regression coefficient was estimated as the ratio of covariance between dimorphism presence and complexity index to the variance of dimorphism presence. Significance of the trait correlation was tested by comparing the harmonic mean of the Bayes factor (BF) from runs under a dependent (correlation allowed) character model to that under an independent (correlation fixed to 0) model. A $\log(BF) > 10$ was considered to give very strong support for the best model. To incorporate phylogenetic uncertainty, the analysis was simulated on 50 trees sampled from the posterior distribution of trees from the phylogenetic analysis. MCMC chains were run for 10 million generations, sampling chains every 1000 generations.

619 **References**

620

621 Andrássy I. 1984. *Klasse Nematoda*. Stuttgart: Fischer Verlag.

622 Andrássy I. 2005. *Free-living nematodes of Hungary, I (Nematoda errantia)*.
623 Budapest: Hungarian National History Museum.

624 Baldwin JG, Giblin-Davis RM, Eddleman CD, Williams DS, Vida JT, Thomas WK.
625 1997. The buccal capsule of *Aduncospiculum halicti* (Nemata: Diplogasterina): an
626 ultrastructural and molecular phylogenetic study. *Canad J Zool* **75**:407-423. doi:
627 10.1139/z97-051

628 Baldwin JM. 1896. A new factor in evolution. *Am Nat* **30**:441-451; 536-553.

629 Barrett RDH, Schluter D. 2008. Adaptation from standing genetic variation. *Trends*
630 *Ecol Evol* **23**:38-44. doi: 10.1016/j.tree.2007.09.008

631 Bento G, Ogawa A, Sommer RJ. 2010 Co-option of the hormone signalling module
632 dafachronic acid-DAF-12 in nematode evolution. *Nature* **466**:494-497. doi:
633 10.1038/nature09164

634 Blaxter ML, De Ley P, Garey JR, Liu LX, Scheldeman P, Vierstraete A, Vanfleteren
635 JR, Mackey LY, Dorris M, Frisse LM, Vida JT, Thomas WK. 1998. A molecular
636 evolutionary framework for the phylum Nematoda. *Nature* **392**:71-75. doi:
637 10.1038/32160

638 Bollback JP. 2006. SIMMAP: stochastic character mapping of discrete traits on
639 phylogenies. *BMC Bioinformatics* **7**:88. doi: 10.1186/1471-2105-7-88

640 Bose N, Ogawa A, von Reuss SH, Yim JJ, Ragsdale EJ, Sommer RJ, Schroeder FC.
641 2012. Complex small-molecule architectures regulate phenotypic plasticity in a
642 nematode. *Angew Chem* **51**:12438-12443. doi: 10.1002/anie.201206797

643 Burnham KP, Anderson DR. 2002. *Model selection and multimodel interference: a*
644 *practical information-theoretic approach*. New York: Springer.

645 Cheverud JM. 1996. Developmental integration and the evolution of pleiotropy. *Am*
646 *Zool* **36**:44-50.

647 Ciampaglio CN, Kemp M, McShea DW. 2001. Detecting changes in morphospace
648 occupation patterns in the fossil record: characterization and analysis measures of
649 disparity. *Palaeobiology* **27**:695-715. doi: 10.1666/0094-
650 8373(2001)027<0695:DCIMOP>2.0.CO;2

651 Darriba D, Taboada GL, Doallo R, Posada D. 2011. ProtTest 3: fast selection of best-
652 fit models of protein evolution. *Bioinformatics* **27**:1164-1165. doi:
653 10.1093/bioinformatics/btr088
654 de Jong G. 2005. Evolution of phenotypic plasticity: patterns of plasticity and the
655 emergence of ecotypes. *New Phytol* **166**:101-118. doi: 10.1111/j.1469-
656 8137.2005.01322.x
657 De Ley P, Blaxter ML. 2002. Systematic position and phylogeny. In: Lee DL, editor.
658 *The Biology of Nematodes*. London: Taylor & Francis.
659 De Ley P, van de Velde MC, Mounport D, Baujard P, Coomans A. 1995.
660 Ultrastructure of the stoma in Cephalobidae, Panagrolaimidae, and Rhabditidae,
661 with a proposal for a revised stoma terminology in Rhabdtida (Nematoda).
662 *Nematologica* **41**:153-182.
663 Drummond AJ, Rambaut A. 2007. BEAST: Bayesian evolutionary analysis by
664 sampling trees. *BMC Evol Biol* **7**:214. doi: 10.1186/1471-2148-7-214
665 Dryden IL, Mardia KV. 1998. *Statistical shape analysis*. Chichester: Wiley.
666 Eastman JM, Alfaro ME, Joyce P, Hipp AL, Harmon LJ. 2011. A novel comparative
667 method for identifying shifts in the rate of character evolution on trees. *Evolution*
668 **65**:3578-3589. doi: 10.1111/j.1558-5646.2011.01401.x
669 Edgar RC. 2004. MUSCLE: multiple sequence alignment with high accuracy and
670 high throughput. *Nucleic Acids Res* **32**:1792-1797. doi: 10.1093/nar/gkh340
671 Emlen DJ, Hunt J, Simmons LW. 2005. Evolution of sexual dimorphism and male
672 dimorphism in the expression of beetle horns: phylogenetic evidence for
673 modularity, evolutionary lability, and constraint. *Am Nat* **166**:S42-S68. doi:
674 10.1086/444599
675 Felsenstein J. 2012. A comparative method for both discrete and continuous
676 characters using the threshold model. *Am Nat* **179**:145-156. doi: 10.1086/663681
677 Fürst von Lieven A. 2000. Vergleichende und funktionelle Morphologie der
678 Mundhöhle der Diplogastrina (Nematoda) mit einem ersten Entwurf der
679 Phylogenie dieses Taxons. Ph. D. dissertation, Freie Universität Berlin.
680 Fürst von Lieven A, Sudhaus W. 2000. Comparative and functional morphology on
681 the buccal cavity of Diplogastrina (Nematoda) and a first outline of the phylogeny
682 of this taxon. *J Zool Syst Evol Res* **38**:37-63. doi: 10.1046/j.1439-
683 0469.2000.381125.x
684

685 Harjunmaa E, Kallonen A, Voutilainen M, Hämäläinen K, Mikkola ML, Jernvall J.
686 2012. On the difficulty of increasing dental complexity. *Nature* **483**:324-327. doi:
687 10.1038/nature10876
688 Harjunmaa E, Seidel K, Häkkinen T, Renvoisé E, Corfe IJ, Kallonen A, Zhang ZQ,
689 Evans R, Mikkola ML, Salazar-Ciudad I, Klein OD, Jernvall J. 2014. Replaying
690 evolutionary transitions from the dental fossil record. *Nature* **512**:44-48. doi:
691 10.1038/nature13613
692 Harmon LJ, Weir J, Brock C, Glor RE, Challenger W. 2008. GEIGER: investigating
693 evolutionary radiations. *Bioinformatics* **24**:129-131. doi:
694 10.1093/bioinformatics/btm538
695 Herrmann M, Mayer WE, Sommer RJ. 2006. Nematodes of the genus *Pristionchus*
696 are closely associated with scarab beetles and the Colorado potato beetle in
697 Western Europe. *Zoology* **109**:96-108. doi: 10.1016/j.zool.2006.03.001
698 Herrmann M, Ragsdale EJ, Kanzaki N, Sommer RJ. 2013. *Sudhausia aristotokia* n.
699 gen., n. sp. and *S. crassa* n. gen., n. sp. (Nematoda: Diplogastridae): viviparous
700 new species with precocious gonad development. *Nematology* **15**:1001-1020. doi:
701 10.1163/15685411-00002738
702 Huelsenbeck JP, Nielsen R, Bollback JP. 2003. Stochastic mapping of morphological
703 characters. *Syst Biol* **52**:131-138. doi: 10.1080/10635150390192780
704 Kanzaki N, Ragsdale EJ, Herrmann M, Sommer RJ. 2012. Two new species of
705 *Pristionchus* (Rhabditida: Diplogastridae): *P. fissidentatus* n. sp. from Nepal and
706 La Réunion and *P. elegans* n. sp. from Japan. *J Nematol* **44**:80-91.
707 Katoh K, Standley DM. 2013. MAFFT multiple alignment software version 7:
708 improvements in performance and usability. *Mol Biol Evol* **30**:772-780. doi:
709 10.1093/molbev/mst010
710 Kawecki TJ. 1994. Accumulation of deleterious mutations and the evolutionary cost
711 of being a generalist. *Am Nat* **144**:833-838. doi: 10.1086/285709
712 Kiontke K, Barrière A, Kolotuev I, Podbilewicz B, Sommer R, Fitch DHA, Félix MA.
713 2007. Trends, stasis, and drift in the evolution of nematode vulva development.
714 *Curr Biol* **17**:1925-1937. doi: 10.1016/j.cub.2007.10.061
715 Kiontke KC, Felix MA, Ailion M, Rockman MV, Braendle C, Pénigault JB, Fitch
716 DHA. 2011. A phylogeny and molecular barcodes for *Caenorhabditis*, with
717 numerous new species from rotting fruits. *BMC Evol Biol* **11**:339. doi:
718 10.1186/1471-2148-11-339

719 Klingenberg CP. 2011. MorphoJ: an integrated software package for geometric
720 morphometrics. *Mol Ecol Resour* **11**:353-357. doi: 10.1111/j.1755-
721 0998.2010.02924.x
722 Lande R. 2009. Adaptation to an extraordinary environment by evolution of
723 phenotypic plasticity and genetic assimilation. *J Evol Biol* **22**:1435-1445. doi:
724 10.1111/j.1420-9101.2009.01754.x
725 Ledón-Rettig CC, Pfennig DW, Crespi EJ. 2010. Diet and hormonal manipulation
726 reveal cryptic genetic variation: implications for the evolution of novel feeding
727 strategies. *Proc R Soc B* **277**:3569-3578. doi: 10.1098/rspb.2010.0877
728 Maddison WP, Maddison DR. 2011. Mesquite: a modular system for evolutionary
729 analysis. Version 2.75. [http://mesquiteproject.org].
730 Mayer WE, Herrmann M, Sommer RJ. 2009. Molecular phylogeny of beetle
731 associated diplogastrid nematodes suggests host switching rather than nematode-
732 beetle coevolution. *BMC Evol Biol* **9**:212. doi: 10.1186/1471-2148-9-212
733 Miller MA, Pfeiffer W, Schwarz T. 2006. Creating the CIPRES Science Gateway for
734 inference of large phylognetic trees. In: *Proceedings of the Gateway Computing*
735 *Environments Workshop (GCE), 14 November*. New Orleans. p 1-8.
736 Mitteroecker P, Gunz P, Bernhard M, Schaefer K, Bookstein FL. 2004. Comparison
737 of cranial ontogenetic trajectories among great apes and humans. *J Hum Evol*
738 **46**:679-698. doi: 10.1016/j.jhevol.2004.03.006
739 Moczek AP, Sultan SE, Foster SA, Ledón-Rettig CC, Dworkin I, Abouheif E, Pfennig
740 DW. 2011. The role of developmental plasticity in evolutionary innovation. *Proc*
741 *R Soc B* **278**, 2705-2713. doi: 10.1098/rspb.2011.0971
742 Moran NA. 1992. The evolutionary maintenance of alternative phenotypes. *Am Nat*
743 **139**:971-989. doi: 10.1086/285369
744 Navarro N. 2003. MDA: a MATLAB-based program for morphospace-disparity
745 analysis. *Comput Geosci* **29**:655-654. doi: 10.1016/S0098-3004(03)00043-8
746 Nielsen R. Mapping mutations on phylogenies. *Syst Biol* **51**:729-739. doi:
747 10.1080/10635150290102393
748 O'Meara BC, Ané C, Sanderson MJ, Wainwright PC. 2006. Testing for different rates
749 of continuous trait evolution using likelihood. *Evolution* **60**:922-933. doi:
750 10.1111/j.0014-3820.2006.tb01171.x
751 Pagel M. 1997. Inferring evolutionary processes from phylogenies. *Zool Scr* **26**:331-
752 348. doi: 10.1111/j.1463-6409.1997.tb00423.x

753 Pagel M, Meade A. 2013. BayesTraits V2 (beta)
754 [http:www.evolution.rdg.ac.uk/BayesTraits.html].
755 Pfennig DW, McGee M. 2010. Resource polyphenism increases species richness: a
756 test of the hypothesis. *Phil Trans R Soc B* **365**:577-591. doi:
757 10.1098/rstb.2009.0244
758 Pigliucci M. 2001. *Phenotypic Plasticity: Beyond Nature and Nurture: Syntheses in*
759 *Ecology and Evolution*. Baltimore: Johns Hopkins University Press.
760 Plummer M, Best N, Cowles K, Vines K, Sarkar D, Almond R. 2012. coda: output
761 analysis and diagnostics for MCMC. R package version 0.16-1. [http://CRAN.R-
762 project.org/package=magic].
763 R Development Core Team. 2013. R: a language and environment for statistical
764 computing. [http://www.R-project.org] In: *R foundation for Statistical Computing*.
765 Vienna.
766 Ragsdale EJ, Baldwin JG. 2010. Resolving phylogenetic incongruence to articulate
767 homology and phenotypic evolution: a case study from Nematoda. *Proc R Soc B*
768 **277**:1299-1307. doi: 10.1098/rspb.2009.2195
769 Ragsdale EJ, Kanzaki N, Sommer RJ. 2014. *Levipalatum texanum* n. gen., n. sp.
770 (Nematoda: Diplogastridae), an androdioecious species from the south-eastern
771 USA. *Nematology* **16**:695-709. doi: 10.1163/15685411-00002798
772 Ragsdale EJ, Müller MR, Rödelsperger C, Sommer RJ. 2013. A developmental
773 switch coupled to the evolution of plasticity acts through a sulfatase. *Cell*
774 **155**:922-933. doi: 10.1016/j.cell.2013.09.054
775 Revell LJ. 2009. Size-correction and principal components for interspecific
776 comparative studies. *Evolution* **63**:3258-3268. doi: 10.1111/j.1558-
777 5646.2009.00804.x
778 Revell LJ. 2012. phytools: an R package for phylogenetic comparative biology (and
779 other things). *Methods Ecol Evol* **3**:217-223. doi: 10.1111/j.2041-
780 210X.2011.00169.x
781 Rohlf FJ. 2008. TpsDig2: a program for landmark development and analysis.
782 Department of Ecology and Evolution, State University of New York at Stony
783 Brook. [http://life.bio.sunysb.edu/morph/].
784 Rohlf FJ, Slice D. 1990. Extensions of the Procrustes method for optimal
785 superimposition of landmarks. *Syst Zool* **39**:40-59. doi: 10.2307/2992207

786 Ronquist F, Teslenko M, van der Mark P, Ayres DL, Darling A, Höhna S, Larget B,
787 Liu L, Suchard MA, Huelsenbeck JP. 2012. MrBayes 3.2: efficient Bayesian
788 phylogenetic inference and model choice across a large model space. *Syst Biol*
789 **61**:539-542. doi: 10.1093/sysbio/sys029
790 Schlichting CD. 2003. Origins of differentiation via phenotypic plasticity. *Evol Dev* **5**,
791 98-105. doi: 10.1046/j.1525-142X.2003.03015.x
792 Scholze VS, Sudhaus W. 2011. A pictorial key to the current genus groups of
793 "Rhabditidae." *J Nematode Morphol Syst* **14**:105-112.
794 Schwander T, Leimar O. 2011. Genes as leaders and followers in evolution. *Trends*
795 *Ecol Evol* **26**:143-151. doi: 10.1016/j.tree.2010.12.010
796 Serobyan V, Ragsdale EJ, Müller MR, Sommer RJ. 2013. Feeding plasticity in the
797 nematode *Pristionchus pacificus* is influenced by sex and social context and is
798 linked to developmental speed. *Evol Dev* **15**:161-170. doi: 10.1111/ede.12030
799 Serobyan V, Ragsdale EJ, Sommer RJ. 2014. Adaptive value of a predatory mouth-
800 form in a dimorphic nematode. *Proc R Soc B* **281**:20141334. doi:
801 10.1098/rspb.2014.1334
802 Snell-Rood EC, Van Dyken JD, Cruickshank T, Wade MJ, Moczek AP. 2010.
803 Toward a population genetic framework of developmental evolution: the costs,
804 limits, and consequences of phenotypic plasticity. *BioEssays* **32**:71-81. doi:
805 10.1002/bies.200900132
806 Stamatakis A. 2006. RAxML-VI-HPC: maximum likelihood-based analyses with
807 thousands of taxa and mixed models. *Bioinformatics* **22**:2688-2690. doi:
808 10.1093/bioinformatics/btl446
809 Sudhaus W. 2011. Phylogenetic systemisation and catalogue of paraphyletic
810 "Rhabditidae" (Secernentea, Nematoda). *J Nematode Morphol Syst* **14**:113-178.
811 Sudhaus W, Fürst von Lieven A. 2003. A phylogenetic classification and catalogue of
812 the Diplogastridae (Secernentea, Nematoda). *J Nematode Morphol Syst* **6**:43-90.
813 Suzuki Y, Nijhout HF. 2006. Evolution of a polyphenism by genetic accommodation.
814 *Science* **311**:650-652. doi: 10.1126/science.1118888
815 Turing AM. 1952. The chemical basis of morphogenesis. *Phil Trans R Soc B* **641**:37-
816 72. doi: 10.1098/rstb.1952.0012
817 Van Dyken JD, Wade MJ. 2010. The genetic signature of conditional expression.
818 *Genetics* **184**:557-570. doi: 10.1534/genetics.109.110163

van Megen H, van den Elsen S, Holterman M, Karssen G, Mooyman P, Bongers T, Holovachov O, Bakker J, Helder J. 2009. A phylogenetic tree of nematodes based on about 1200 full-length small subunit ribosomal DNA sequences. *Nematology* **11**:927-950. doi: 10.1163/156854109X456862

Waddington CH. 1953. Genetic assimilation of an acquired character. *Evolution* **7**:118-126. doi: 10.2307/2405747

Weller AM, Rödelsperger C, Eberhardt G, Molnar RI, Sommer RJ. 2014. Opposing forces of A/T-biased mutations and G/C-biased gene conversions shape the genome of the nematode *Pristionchus pacificus*. *Genetics* **196**:1145-1152. doi: 10.1534/genetics.113.159863

West-Eberhard MJ. 1986. Alternative adaptations, speciation, and phylogeny (a review). *Proc Natl Acad Sci USA* **83**:1388-1392. doi: 10.1073/pnas.83.5.1388

West-Eberhard MJ. 2003. *Developmental plasticity and evolution*. Oxford: Oxford University Press.

Williams GC. 1966. *Adaptation and natural selection*. Princeton: Princeton University Press.

Wund MA. 2012. Assessing the impacts of phenotypic plasticity on evolution. *Int Comp Biol* **52**:5-15. doi: 10.1093/icb/ics050

838 **Figure legends**

839

840 **Figure 1. Mouth dimorphism and novelty in Diplogastridae.** (**A**) The diplogastrid
841 eurystomatous (Eu) morph, as shown here for *Parapristionchus giblindavisi*, is
842 marked by a wider mouth, larger teeth, and often greater stomatal complexity than the
843 stenostomatous (St) morph. (**B**) *P*. *giblindavisi*, St morph. False coloring in (**A**,**B**)
844 indicates individual cuticular compartments of the mouth, providing a basis for
845 tracking changes in homologous structures (yellow, cheilostom; blue, gymnostom;
846 red, stegostom except telostegostom). View in (**A**,**B**) is right lateral and at same scale.
847 Scale bar, 10 μm. **c**, Opposing teeth, shown here for *Fictor* sp. 1, are a structural
848 novelty of Diplogastridae and used for predatory feeding. Visible serrated plates are
849 among other feeding innovations of Diplogastridae. Dorsal is right; scale bar, 5 μm.

850

851 **Figure 2. A radiation of feeding structures in diplogastrid nematodes.** (**A**)
852 Phylogenetic relationships inferred for nematodes of Rhabditina, including 54 species
853 of Diplogastridae (Figure 2-source data 1, 2) from an alignment including SSU rRNA,
854 LSU rRNA, and 11 ribosomal protein genes (for Diplogastridae, 468 kb excluding
855 missing data), and RNA polymerase II. History of dimorphism inferred by stochastic
856 character mapping on the set of sampled Bayesian posterior trees (consensus tree is
857 shown). **, 100% posterior probability (PP); *, 99% PP. (**B**) Morphological diversity
858 of mouthparts in Diplogastridae (light blue and white blocks), which are strikingly
859 complex with respect to outgroups (yellow block). The origin of plasticity coincided
860 with a radiation of complex feeding-forms, which variously include opposing teeth,
861 bilateral asymmetry, and additional armature and articulations. In shape, form, and
862 complexity, the mouths of outgroups (*Ri*, *Ce*, *Hb*) are more similar to the St than the
863 Eu morph of dimorphic species. For dimorphic taxa, Eu morph is shown. Two-letter
864 designations abbreviate Linnaean binomials of depicted species.

865

866 **Figure 3. Developmental plasticity, morphological disparity, and evolutionary**
867 **tempo in diplogastrid nematodes.** (**A**), Stomatal morphology and positions of 11
868 two-dimensional landmarks (taxa coded in Figure 2). Below is a projection of the first
869 two principal components of stomatal shape-space. Purple circles represent non-
870 diplogastrid Rhabditina (Rh), green circles mark monomorphic Diplogastridae (Mn);
871 blue and red circles connected by lines mark St and Eu morphs, respectively, of

dimorphic Diplogastridae. (**B**) Phenotypic disparity of non-diplogastrid Rhabditina (Rh), Diplogastridae (Dip, dimorphic taxa are represented by St morph; Dip*, by both morphs), and individually of St, Eu, and monomorphic (Mn) Diplogastridae, as estimated by the sum of variances on shape- and form-space axes. Bars show mean values from 10,000 bootstrap replicates. Whiskers represent a 95% confidence interval. (**C**) Model-averaged relative estimates of evolutionary rates, as estimated under a Brownian motion model. Both a two-rate model (left) and a three-rate model (right) are shown (Dm, dimorphic Diplogastridae as represented by St morph). Bars are mean rates calculated across 5,000 reconstructions of dimorphism history and 500 trees. Whiskers represent the standard deviation. (**D**) Rate estimates of stomatal form evolution in Rhabditina. In dimorphic taxa, rates are for St morph. Branch color indicates rates of evolutionary change; posterior rates are color-coded in legend.

Figure 4. **Correlation of polyphenism and complexity of nematode mouthparts.** Painted branches show congruence of simulated character histories of dimorphism (right tree; 0 = absent, 1 = present) and stomatal complexity (left tree; complexity index ranges from 0 to 9). Covariance tests (see text) show that the apparent phylogenetic correlation between dimorphism and complexity is significant.

Table 1. Environmental regulation of the mouth dimorphism across Diplogastridae. The presence of prey nematode (*C. elegans*) larvae and the absence of bacterial food ("prey" treatment) induced development of the Eu morph in strains normally St-biased on an abundance of bacterial food (control). For species that could not reach adulthood on this regimen, conditions of overpopulation and starvation ("starved" treatment) similarly promoted the Eu morph. Effect size is given as the odds ratio (Fisher's exact test) where not infinite.

Dimorphic nematode species	Treatment type	% Eu, treatment	% Eu, control	Odds ratio
Allodiplogaster sp. 1	prey	100	0	
Allodiplogaster sudhausi	prey	97	1	1080.976
Diplogasteriana n. sp.	starved	24	0	
Fictor stercorarius	prey	96	0	
Koerneria luziae	starved	5	0	
Micoletzkya inedia	prey	95	0	
Micoletzkya japonica	prey	92	0	
Mononchoides sp. 1	prey	98	10	120.272
Mononchoides sp. 3	prey	100	6	
Neodiplogaster sp.	prey	100	0	
Parapristionchus giblindavisi	starved	34	6	8.428

Supplementary figure, source data, and data file legends

Table 1-source data 1. Environmental induction of the Eu morph in dimorphic species. Results for individual replicates (plates) are shown.

Figure 2-source data 1. Nematode taxa used in this study, with isolation details given. Origins of strains are coded as follows: CGC, Caenorhabditis Genetics Center; JB, Baldwin lab (U. California, Riverside); MV, Viney lab (U. Bristol); NK, Kanzaki lab; RGD, Giblin-Davis lab (U. Florida-IFAS); RS, Sommer lab; SB, Sudhaus lab (Freie Universität Berlin). For other strains, references are given. nc, not culturable.

Figure 2-source data 2. GenBank accession numbers for gene sequences analyzed in this study. Sequences shorter than 200 bp (with accession numbers beginning with "VS") are available at www.pristionchus.org/download/suppSusoy2014.html.

Figure 3-figure supplement 1. Projections of the first two principal components of Procrustes morphospace of stomatal landmarks. In phylogenetic principal components analysis (phylogenetic PCA), dimorphic species are represented by the St morph. Purple circles represent non-diplogastrid Rhabditina (Rh), green circles mark monomorphic Diplogastridae (Mn); red circles, St morph of dimorphic Diplogastridae; blue and red circles connected by lines mark St and Eu morphs of individual dimorphic species. (**A**) Phylogenetic PCA of form. (**B**) Phylogenetic PCA of shape. (**C**) PCA of shape.

Figure 3-figure supplement 2. Rate estimates of stomatal shape evolution in Rhabditina. In dimorphic taxa, rates are for St morph. Branch color indicates rates of evolutionary change; posterior rates are color-coded in legend.

Figure 3-figure supplement 3. Posterior densities of rates of stomatal form and shape evolution in Rhabditina. Bars below represent highest posterior density intervals of weighted rate estimates for the groups. Rh, non-diplogastrid Rhabditina; Dm, dimorphic Diplogastridae; Mn, monomorphic Diplogastridae. (**A**) Rates of change of Procrustes form. (**B**) Rates for Procrustes shape. Results from analyses of form show both groups of Diplogastridae to have higher rates than monomorphic outgroups, although rates were highest in secondarily monomorphic lineages.

936 Analyses of shape also clearly show higher rates in Diplogastridae as compared with
937 outgroups.
938
939 **Figure 3-source data 1. Results of principal component analysis ofstomatal form**
940 **in Rhabditina, including both morphs of dimorphic taxa.** Loadings of Procrustes
941 coordinates and log centroid size of stomatal form onto the first four principal
942 component (PC) axes are shown, as are the proportion of variance explained by those
943 PC axes.
944
945 **Figure 3-source data 2. Results of principal component analysis of stomatal**
946 **shape in Rhabditina, including both morphs of dimorphic taxa.** Loadings of
947 Procrustes coordinates of stomatal shape onto the first four principal component (PC)
948 axes are shown, as are the proportion of variance explained by those PC axes.
949
950 **Figure 3-source data 3. Results of phylogenetic principal component analysis of**
951 **stomatal form in Rhabditina, with dimorphic taxa represented by the**
952 **stenostomatous (St) morph.** Loadings of Procrustes coordinates and log centroid
953 size of stomatal form onto the first four principal component (PC) axes are shown, as
954 are the proportion of variance explained by those PC axes.
955
956 **Figure 3-source data 4. Results of phylogenetic principal component analysis of**
957 **stomatal shape in Rhabditina, with dimorphic taxa represented by the**
958 **stenostomatous (St) morph.** Loadings of Procrustes coordinates of stomatal shape
959 onto the first four principal component (PC) axes are shown, as are the proportion of
960 variance explained by those PC axes.
961
962 **Figure 3-source data 5. Estimates of morphological disparity of the stoma in**
963 **Rhabditina.** Groups compared were non-diplogastrid Rhabditina, monomorphic
964 Diplogastridae, and dimorphic Diplogastridae. Disparity was measured as the
965 principal component (PC) analysis volume and the sum of univariate variances. PC
966 scores along the first two and three PC axes of Procrustes form and shape space,
967 respectively, were used and are presented in the form mean±standard deviation (95%
968 confidence interval). Eu, eurystomatous; St, stenostomatous.
969

Figure 3-source data 6. Rates of stomatal evolution along the first principal component (PC) axis of Procrustes form- and shape-space. Rates were compared for non-diplogastrid Rhabditina (Rh), dimorphic Diplogastridae (Dm), and monomorphic Diplogastridae (Mn). Numbers indicate separate rate parameters for the designated groups. Model-averaged rates with standard deviation are shown.

Figure 3-source data 7. Statistical comparison of non-nested models of stomatal evolution along the first principal component (PC) axis of Procrustes form- and shape-space using a chi-square distribution. Numbers indicate separate rate parameters for the designated groups. Rh, non-diplogastrid Rhabditina (Rh); Dm, dimorphic Diplogastridae; Mn, monomorphic Diplogastridae.

Figure 3-source data 8. Highest posterior densities (HPD) of rates, and associated p-values obtained from two-tailed randomization tests, of stomatal form and shape evolution. Tests were performed for the branches assigned to non-diplogastrid Rhabditina, dimorphic Diplogastridae, and monomorphic Diplogastridae. CI, confidence interval.

Figure 4-figure supplement 1. Tabulating complexity of nematode mouthparts. The complexity index (ci) was tabulated as the sum of all stomatal "structures," i.e. geometric deviations marked by a <135º vertex from the cylindrical walls of the stoma or from the arched anterior margins of the pharyngeal radii. Tabulated structures are false-colored on illustrations of four example species. Iterative structures and bilaterally symmetrical duplicates were scored as a single structure due to their co-dependence. All aspects are left and lateral unless otherwise specified. Color-coded structures are recorded in Figure 4-source data 1: red, dorsal tooth; pink, right subdorsal denticle; orange, left subventral tooth; yellow, dorsal, basal stegostomatal fold; mauve, gymnostomatal serratae (iterative); dark green, articulated apodeme (bilaterally symmetrical); light blue, radial cheilostomatal divisions (iterative); teal, subventral stegostomatal warts (iterative); purple, left subventral ridge. (**a**) *Mononchoides* sp. 3 (ci = 8), right lateral aspect. An additional structure (pro- and mesostegostomatal serratae) is not observable from this aspect. (**b**) *Paroigolaimella micrura* (ci = 3). (**c**) *Koerneria luziae* (ci = 4). (**d**) *Fuchsnema halleri* (ci = 1).

Figure 4-source data 1. Matrix of structures tabulated to measure stomatal complexity. Structures were recorded as described in text. Presence/absence of dimorphism is also given. 0 = absence, 1 = presence.

Supplementary file 1. Two tree files and a multiple sequence alignment file.

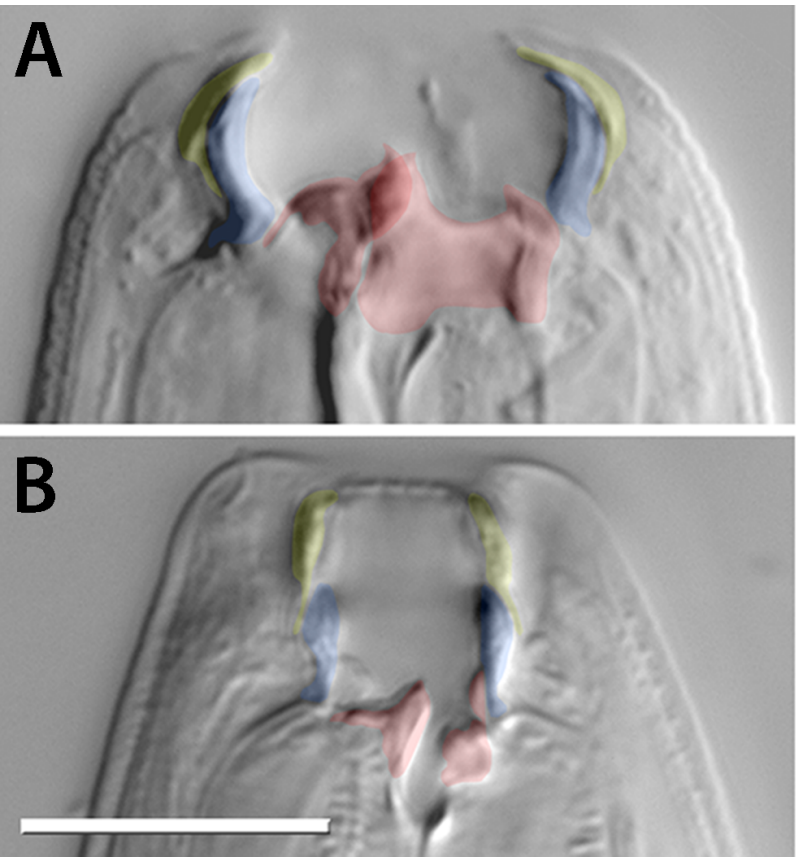
A
B

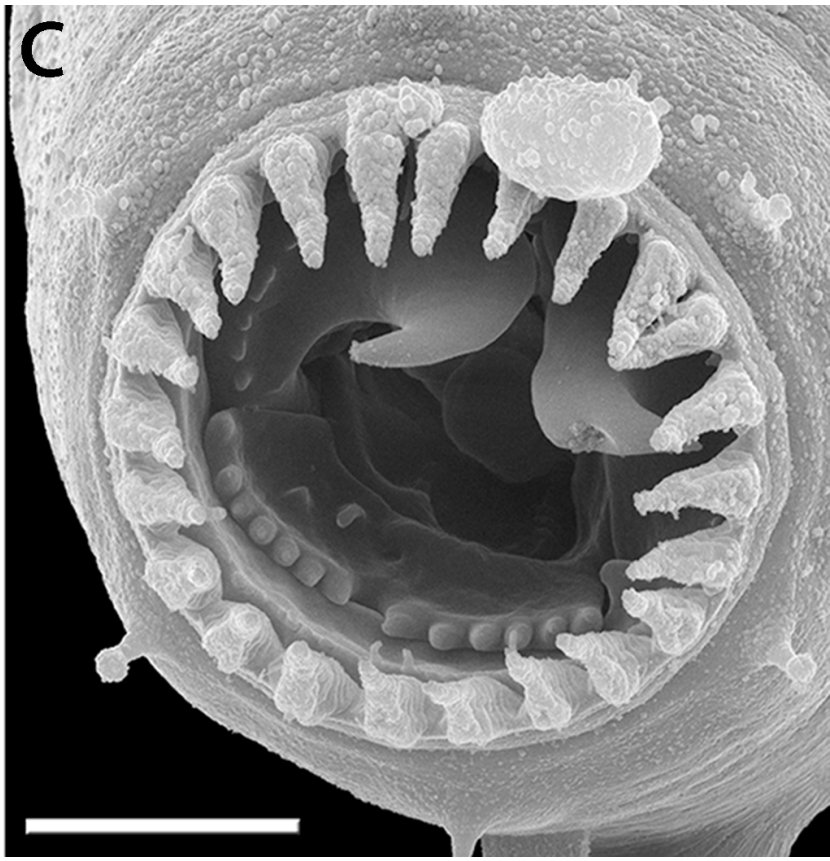
C

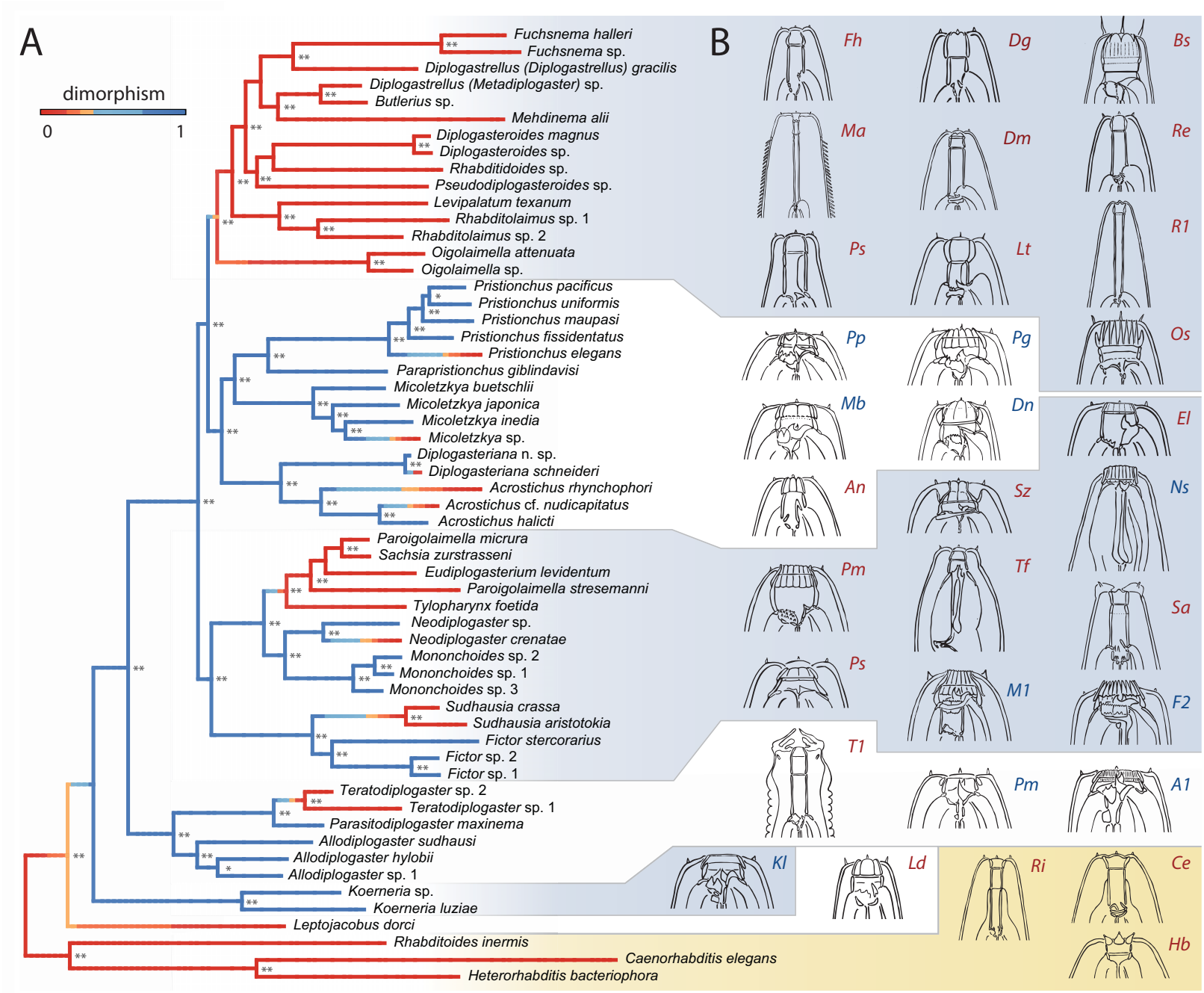
A
dimorphism
0
1
Fuchsnema halleri
Fuchsnema sp.
Diplogastrellus (Diplogastrellus) gracilis
Diplogastrellus (Metadiplogaster) sp.
Butlerius sp.
Mehdinema alii
Diplogasteroides magnus
Diplogasteroides sp.
Rhabditidoides sp.
Pseudodiplogasteroides sp.
Levipalatum texanum
Rhabditolaimus sp. 1
Rhabditolaimus sp. 2
Oigolaimella attenuata
Oigolaimella sp.
Pristionchus pacificus
Pristionchus uniformis
Pristionchus maupasi
Pristionchus fissidentatus
Pristionchus elegans
Parapristionchus giblindavisi
Micoletzkya buetschlii
Micoletzkya japonica
Micoletzkya inedia
Micoletzkya sp.
Diplogasteriana n. sp.
Diplogasteriana schneideri
Acrostichus rhynchophori
Acrostichus cf. nudicapitatus
Acrostichus halicti
Paroigolaimella micrura
Sachsia zurstrasseni
Eudiplogasterium levidentum
Paroigolaimella stresemanni
Tylopharynx foetida
Neodiplogaster sp.
Neodiplogaster crenatae
Mononchoides sp. 2
Mononchoides sp. 1
Mononchoides sp. 3
Sudhausia crassa
Sudhausia aristotokia
Fictor stercorarius
Fictor sp. 2
Fictor sp. 1
Teratodiplogaster sp. 2
Teratodiplogaster sp. 1
Parasitodiplogaster maxinema
Allodiplogaster sudhausi
Allodiplogaster hylobii
Allodiplogaster sp. 1
Koerneria sp.
Koerneria luziae
Leptojacobus dorci
Rhabditoides inermis
Caenorhabditis elegans
Heterorhabditis bacteriophora
B
Fh
Dg
Bs
Ma
Dm
Re
Ps
Lt
R1
Pp
Pg
Os
Mb
Dn
El
An
Sz
Ns
Pm
Tf
Sa
Ps
M1
F2
T1
Pm
A1
Kl
Ld
Ri
Ce
Hb

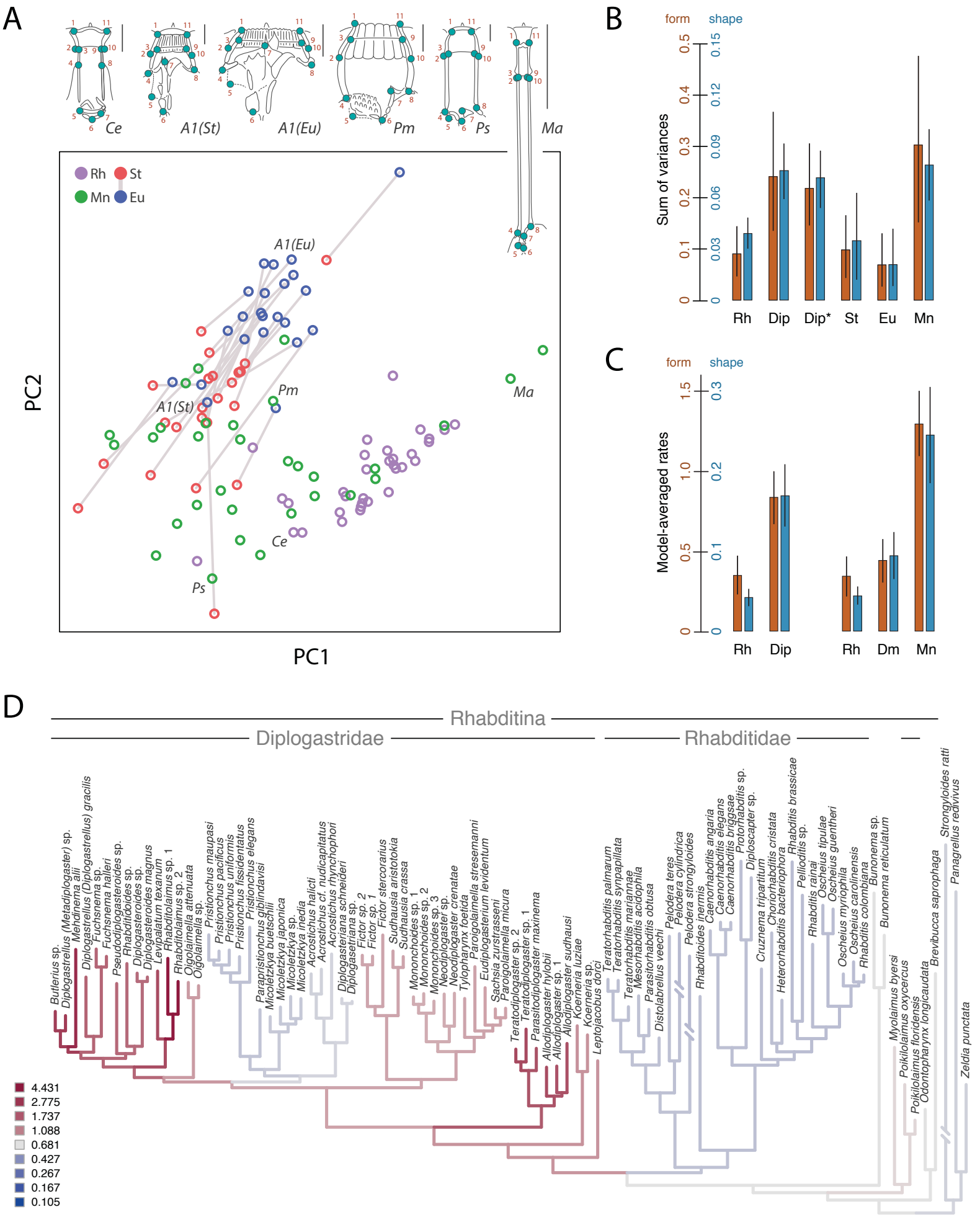
A
Ce
A1(St)
A1(Eu)
Pm
Ps
Ma
Rh
St
Mn
Eu
PC2
PC1
B
form
shape
Sum of variances
Rh
Dip
Dip*
St
Eu
Mn
C
form
shape
Model-averaged rates
Rh
Dip
Rh
Dm
Mn
D
Rhabditina
Diplogastridae
Rhabditidae
4.431
2.775
1.737
1.088
0.681
0.427
0.267
0.167
0.105

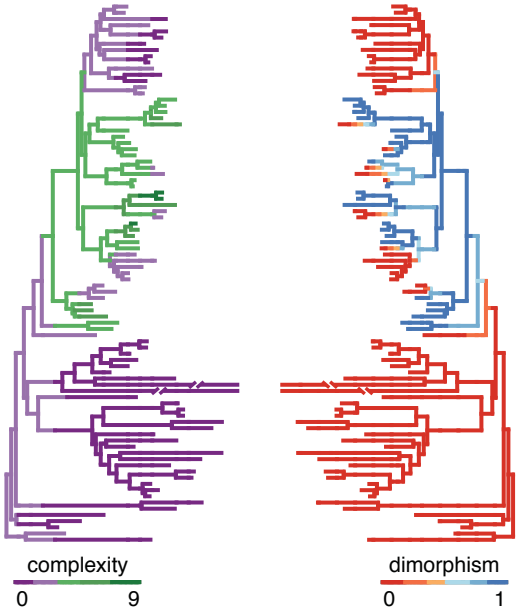
complexity
0
9
dimorphism
0
1